High-pressure polymorphism of the copper(I) halides: A neutron-diffraction study to ~10 GPa

S. Hull and D. A. Keen
ISIS Science Division, Rutherford Appleton Laboratory, Chilton, Didcot, Oxfordshire, OX11 0QX, United Kingdom
(Received 23 March 1994)

The structural changes within the copper(I) halides induced by hydrostatic pressure have been investigated using the powder neutron-diffraction technique. The expected transition from the ambient zinc-blende structure with tetrahedral coordination to the octahedrally coordinated rocksalt structure is observed in both CuCl and CuBr. No rocksalt phase is observed in CuI, presumably due to the limited maximum pressure of our apparatus (~10 GPa). The lower symmetry phases which occur as intermediate structures between the zinc-blende and rocksalt phases have been studied in detail. CuCl and CuI undergo abrupt transitions whilst CuBr has three sluggish transitions, involving extensive coexistence of neighboring phases. There is one intermediate phase in CuCl (CuCl-IV), two in CuBr (CuBr-IV and CuBr-V) and at least two in CuI (CuI-IV and CuI-V). Three different structure types have been identified, in space groups $Pa\bar{3}$ (CuCl-IV and CuBr-V), $P4/nmm$ (CuBr-IV and CuI-V) and $R\bar{3}m$ (CuI-IV). The intermediate structures all retain the tetrahedral cation coordination of the Cu^+, though the environment is rather more distorted in CuCl and CuBr than in CuI. The evolution of the structures of these I-VII compounds is very different from that observed in the more covalent II-VI and III-V systems.

I. INTRODUCTION

At ambient conditions the three copper(I) halides CuCl, CuBr, and CuI all possess the zinc-blende structure (space group $F\bar{4}3m$). Together with AgI, they can be considered as the last members of the series of tetrahedrally coordinated semiconductors which comprises the group IV elements and the III-V, II-VI, and I-VII compounds. The bonding is purely covalent in the group IV elements and the degree of ionicity increases with increasing separation of the constituent elements in the periodic table. On the Phillips scale,[1] these I-VII compounds have ionicities $f \sim 0.7$. This is very close to the critical value $f_c = 0.785$ which marks the idealized boundary between compounds characterized by fourfold-coordinated structures (zinc blende, wurtzite) and those with sixfold coordination (rocksalt). Indeed, AgCl and AgBr crystallize in the rocksalt structure under ambient conditions. Furthermore, AgI, CuCl, CuBr, and CuI might be expected to transform from zinc blende to rocksalt under hydrostatic pressure, since compression favors transitions to more densely packed structures.

The available experimental evidence[2-4] suggests that all three Cu(I) halides adopt the rocksalt structure at pressures in the region of ~10 GPa. However, the p-T phase diagrams have been extensively studied using optical,[5-9] resistivity,[3,4,8] differential thermal analysis,[10] extended x-ray absorption fine structure (EXAFS),[11] Raman scattering,[12] and diffraction[2-4,14,15] techniques and have been summarized by Merrill[16] (Figs. 1–3). These indicate that the transition from fourfold to sixfold coordination occurs via several intermediate phases of apparently lower symmetry, despite the simple geometric relationship between the zinc-blende and rocksalt structures (both consist of interpenetrating cubic close-packed sublattices but displaced by $(\frac{1}{4},\frac{1}{4},\frac{1}{4})$ and $(\frac{1}{2},\frac{1}{2},\frac{1}{2})$, respectively). Attempts to organize the high-pressure behavior of the Cu(I) halides in relation to that of AgI and the III-V and II-VI compounds[17] have met with serious difficulties, principally because the structures of many of the high-pressure phases are poorly characterized.

Several x-ray diffraction investigations have been reported[2-4,18,19] but the available structural information is generally unreliable and often contradictory. Other techniques such as EXAFS,[11] Raman scattering,[12] and band-structure calculations[9] have also failed to elucidate the structures. This situation is surprising given the widespread interest in the high-pressure behavior of the Cu(I) halides, which includes their electrical properties [driven by claims of high-temperature superconductivity in CuCl (Refs. 20–22)], the complex behavior of the optical properties[7,9] and evidence of pressure-induced disproportionation[19] (i.e., $2CuBr \rightarrow Cu + CuBr_2$). The high degree of structural uncertainty in these compounds has

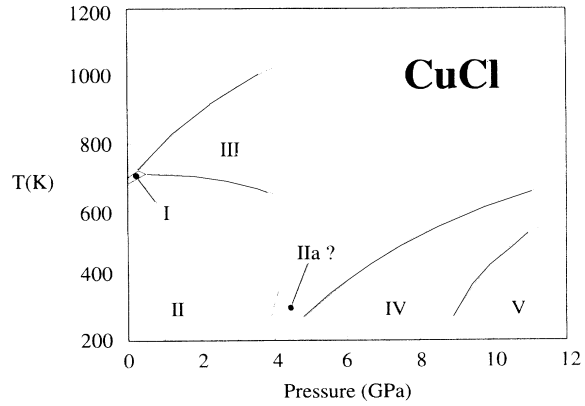

FIG. 1. The p-T phase diagram of CuCl after Merrill (Ref. 16) and including the proposed insulator→metal transition at $p \sim 4$ GPa.

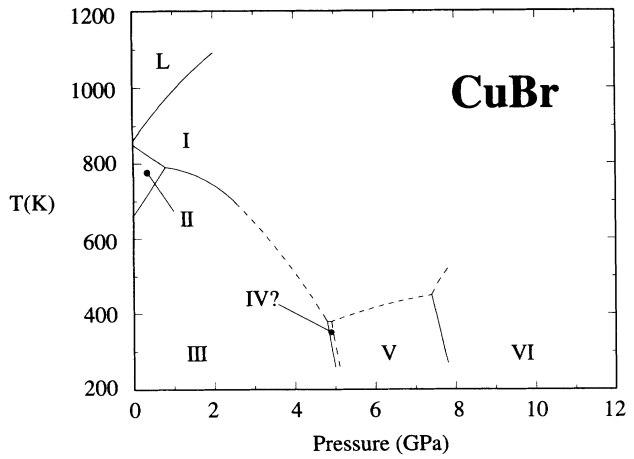

FIG. 2. The p-T phase diagram of CuBr after Merrill (Ref. 16).

prompted this reexamination of the Cu(I) halides using high-pressure neutron powder diffraction.

II. EXPERIMENTAL DETAILS

Commercially available Cu(I) halides supplied by the Aldrich Chemical Co. were used in all measurements, with stated purity 99.995+% (CuCl), 99.999% (CuBr), and 99.999% (CuI). The high-pressure experiments were performed using an opposed anvil pressure cell with a sample volume of ~ 100 mm^3. Details of this device have been given elsewhere.[23] Solid pellets were formed by pressing finely ground material to ~ 0.1 GPa. This operation was performed under subdued lighting and in an argon atmosphere because these compounds (especially CuCl) are sensitive to light and moist air. The pellets were then immediately loaded into the pressure cell, which was then clamped shut to provide an effective seal against the atmosphere. Any brief contact with air during the loading procedure effects the outer surface of the pellet which does not form part of the measured scattering volume of the sample.

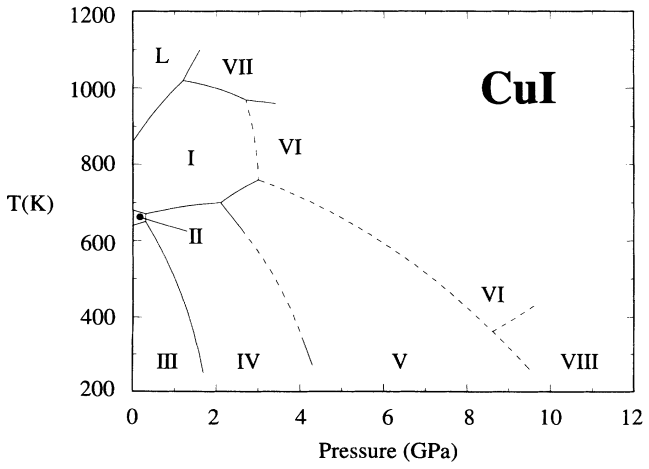

FIG. 3. The p-T phase diagram of CuI after Merrill (Ref. 16).

Diffraction measurements were carried out on the Polaris diffractometer[24] at the ISIS spallation neutron source, U.K., using ZnS scintillator detectors situated at scattering angles in the range $82° < \pm 2\theta < 98°$. These provide diffraction data using the time-of-flight method over the d-spacing range 0.3 Å $< d <$ 4.3 Å. The resolution is $\Delta d/d \sim 0.6\%$ and essentially independent of d. Corrected data is obtained by subtraction of the essentially featureless pattern measured from the empty pressure cell, followed by removal of the wavelength dependence of the incident neutron flux and the effects of attenuation of the incident and scattered beams by the pressure cell components. Rietveld profile refinements of the time-of-flight diffraction data used the computer program TF12LS (Ref. 25) and its multiphase derivative, which are based on the Cambridge Crystallographic Subroutine Library.[26]

Table I demonstrates the lack of agreement concerning the transition pressures in the three Cu(I) halides. These principally result from inconsistencies in the pressure calibration and, therefore, the method used in this study is described in some detail here. Initial diffraction measurements of an approximate one hour duration were made using each Cu(I) halide in turn, intimately mixed with NaCl of purity 99.999%. Least-squares refinement of the diffraction data gives accurate values of the lattice parameters of both NaCl and the sample, to a relative precision of $\sim 10^{-4}$. The former determines the pressure using the equation of state of NaCl given by Decker[27] (accepted to be accurate to ~ 0.05–0.1 GPa in the range 0–10 GPa). The latter then gives the equation of state of the Cu(I) halide. Additional information describing the positional and thermal vibration parameters can also be derived from this data but more accurate values for these parameters are obtained from measurements of higher statistical quality, collected from a pure sample. In this case, the sample pressure is determined using the measured cell parameters and the previously determined equation of state. The above procedure can only be applied if the crystal structure of the Cu(I) halide phase is known. Determination of the structure (at an initially unknown pressure) also requires diffraction data of high statistical quality, collected for ~ 12 h. This reduces possible ambiguities in the assignment of both the unit cell and space group. The weak reflections, often unobserved in the previous x-ray-diffraction studies, are of particular importance in this regard.

The quality of the fit to the experimental data is assessed using the usual χ^2 statistic defined as

$$\chi^2 = \frac{R_{\rm wp}^2}{R_{\rm exp}^2} , \tag{1}$$

where the weighted profile R factor, $R_{\rm wp}$ is given by

$$R_{\rm wp}^2 = \sum_{N_d} \frac{(y_{\rm obs} - y_{\rm calc})^2}{(\sigma y_{\rm obs})^2} \Big/ \sum_{N_d} \frac{(y_{\rm obs})^2}{(\sigma y_{\rm obs})^2} \tag{2}$$

and the summations are made over the N_d data points used in the fit. The expected R factor, $R_{\rm exp}$ is then given by

$$R^2_{\text{exp}} = (N_d - N_p) \Big/ \sum_{i=1}^{N_d} \frac{(y_{\text{obs}})^2}{(\sigma y_{\text{obs}})^2} , \quad (3)$$

where N_p is the number of fitted parameters. y_{obs} and y_{calc} are the observed and calculated intensities, respectively, and σy_{obs} is the estimated standard deviation on y_{obs} derived from the counting statistics.

III. RESULTS

Prior to discussing the results for each compound individually three general points can be made. All measurements presented in this paper were made on compression. The opposed anvil cell generates pressure by plastic deformation on a TiZr alloy gasket surrounding the sample,[23] which generally fails on decompression. Secondly, all post-pressure samples had the zinc-blende structure and there is no evidence for quenched high-pressure phases. Finally, within the time scales of the diffraction measurements, no significant structural changes are observed with time, even for data collected in a pressure range where two phases coexist.

Interpretation of the rather complex behavior of CuBr relies on the results obtained for CuI and CuCl so this compound is described last. For each compound we first discuss the transition pressures, followed by structural

TABLE I. Summary of the published literature describing the pressure-induced phase transitions in CuCl, CuBr, and CuI. The transition CuCl-II→CuCl-IIa is the controversial insulator→metal transition associated with possible high-temperature superconductivity in CuCl.

	CuCl-II→CuCl-IIa		CuCl-II→CuCl-IV		CuCl-IV→CuCl-V	
CuCl	p_{trans} (GPa)	$\Delta V/V_0$ (%)	p_{trans} (GPa)	$\Delta V/V_0$ (%)	p_{trans} (GPa)	$\Delta V/V_0$ (%)
Optical (Ref. 5)			5.4		10.0	
Optical (Ref. 6)			4.2			
X-ray diffraction (Ref. 2)			5.2	10	6.0	1
X-ray/Resistivity (Ref. 4)	4.2		5.5	11.5	10.0	1.5
X-ray diffraction (Ref. 18)			5.3	12	10.5	1
X-ray/Resistivity (Ref. 3)			4.4	11	8.2	0.9
X-ray diffraction (Ref. 13)			5.5	12		
Optical (Ref. 7)			5.0		9.0	
Optical/Resistivity (Ref. 8)			5.1(1)		8.8(4)	
Optical (Ref. 9)	4.2		5.0		~10.5	
Neutron diffraction[a]			5.1(1)	6.71(2)	10.6(3)	2.71(2)
	CuBr-III→CuBr-IV		CuBr-IV→CuBr-V		CuBr-V→CuBr-VI	
CuBr	p_{trans} (GPa)	$\Delta V/V_0$ (%)	p_{trans} (GPa)	$\Delta V/V_0$ (%)	p_{trans} (GPa)	$\Delta V/V_0$ (%)
Optical (Ref. 5)	b	b	5.0		8.0	
Optical (Ref. 6)	b	b	4.7		8.0	
X-ray diffraction (Ref. 2)	b	b	5.0	13	6.6	1
Optical (Ref. 7)	b	b	5.0		7.4	
Optical (Ref. 9)	b	b	5.0		9.0	
EXAFS (Ref. 11)	b	b	4.6(5)		6.4–8.5	
Neutron diffraction[a]	4.8–5.2	5.94(2)	5.0–7.2	1.08(1)	7.4–9.3	4.49(2)
	CuI-III→CuI-IV		CuI-IV→CuI-V		CuI-V→CuI-VIII	
CuI	p_{trans} (GPa)	$\Delta V/V_0$ (%)	p_{trans} (GPa)	$\Delta V/V_0$ (%)	p_{trans} (GPa)	$\Delta V/V_0$ (%)
Volumetric (Ref. 28)	1.0–1.5					
Optical (Ref. 5)	1.4		4.1		8.0	
Optical (Ref. 6)	1.5					
X-ray diffraction (Ref. 14)	1.4–2.5	3.96	5.3–6.0			
X-ray diffraction (Ref. 2)	1.5	4	4.2	1	8.0	10
Raman scattering (Ref. 12)	1.4–1.5		3.9–4.1			
Optical (Ref. 7)	1.8		4.6		9.0	
Optical (Ref. 9)	1.4		3.3		>7.5	
Neutron diffraction[c]	1.63(1)	4.1(1)	4.70(5)	1.11(3)	>9.69	

[a]Work presented in this paper.
[b]Transitions CuBr-III→CuBr-IV and CuBr-IV→CuBr-V either not seen or could not be isolated and are treated as a single transition with the values given in the following columns.
[c]Work presented in Ref. 15 and in this paper.

descriptions of the various phases. Earlier studies are summarized and, where possible, their findings are reinterpreted in the light of this work.

A. Copper (I) iodide

The observation of a pressure-induced structural phase transition in CuI was made by Bridgman[28] in 1916, who observed a volume discontinuity at $p \sim 1.0-1.5$ GPa. Subsequent measurements using x-ray diffraction[2,14] and optical absorption[5,6] techniques confirmed the presence of the transition CuI-III→CuI-IV at $p \sim 1.5$ GPa (see Table I). The evolution of the neutron-diffraction pattern of CuI with pressure is illustrated in Fig. 4 by data collected using a mixed CuI+NaCl sample. The appearance of additional weak peaks at $d \sim 2.28$ and ~ 2.70 Å characterize the transition to phase CuI-IV. However, in this experiment only limited data is collected in this pressure range because the transition pressure $p = 1.63(1)$ GPa was determined in our previous neutron-diffraction study.[15] On increasing pressure a second instantaneous change in the diffraction pattern occurs at $p = 4.70(5)$ GPa, marked by the appearance of a new reflection at $d \sim 2.55$ Å and the disappearance of the lines associated with CuI-IV. There appears to be minimal coexistence of the neighboring phases. With reference to Table I, the observed change is associated with the transition CuI-IV→CuI-V. Several attempts to observe the next transition from CuI-V→CuI-VIII were made in this study, though no change in the diffraction pattern of phase CuI-V was observed up to the maximum pressure possible with this apparatus ($p = 9.69$ GPa with a CuI sample). It is concluded that the CuI-V→CuI-VIII transformation takes place at pressures in the region of 10 GPa or above.

It has been suggested[2] that the poor agreement between the literature values for the CuI-V→CuI-VIII transition pressure arise from the proximity of the stability range of CuI-VI to ambient temperature (see Fig. 3). Indeed, CuI-VI is known to form at ~400 K and ~8 GPa and can partly be retained under ambient conditions.[2] In this work, there is no evidence for phase CuI-VI within the pressure range of CuI-V. Similarly, no effects associated with the controversial anomalies within zinc blende CuI-III at $p \sim 0.4$ GPa and ~0.5 GPa, observed originally by Van Valkenburg,[6] are seen. Support for these transitions was found in bulk compressibility measurements[29] and in x-ray diffraction studies,[30] though the latter could not elucidate their structural consequences. Conversely, no evidence for anomalous behavior was seen in other x-ray diffraction studies[2,14] or in differential scanning calorimetry[10] and eutron-diffraction[15] investigations.

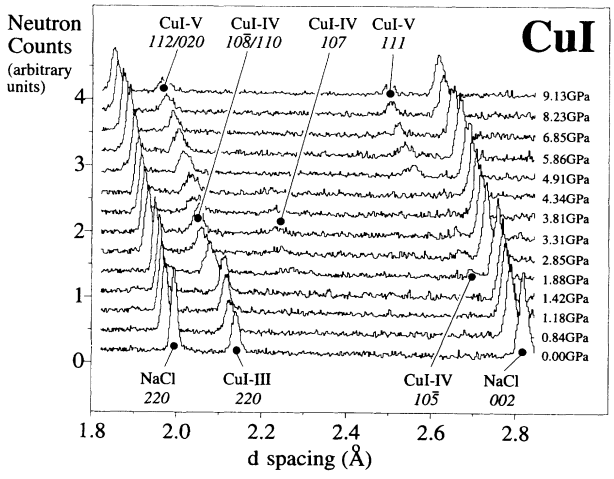

FIG. 4. Evolution of the diffraction pattern of the mixed CuI+NaCl sample with pressure. The structural phase transitions CuI-III→CuI-IV and CuI-IV→CuI-V are observed at $p \sim 1.6$ and ~4.5 GPa, respectively.

Phase CuI-IV

The structural study of CuI at elevated pressures by Moore, Kasper, and Bundy[14] suggested that phase CuI-IV adopts a cubic superstructure of zinc-blende with $a = 11.627$ Å at $p = 3.3$ GPa. Meisalo and Kalliomäki[2] subsequently indexed an x-ray diffraction pattern from CuI-IV at $p = 1.6$ GPa with a hexagonal cell, with $a = 4.164$ Å and $c = 20.41$ Å and containing six formula units. However, their proposed structure with $R3m$ symmetry gave a poor agreement with our recent measurements using powder neutron diffraction. The correct structure has all the Cu^+ in a single, more regular tetrahedron in space group $R\bar{3}m$.[15] CuI-IV has Cu^+ atoms in the 6*c* positions at $(0,0,z_{Cu})$, etc. with $z_{Cu} \sim 0.128$ and the I^- are located in two symmetry independent sites, in 3*a* at (0,0,0), etc., and in 3*b* at $(0,0,\frac{1}{2})$, etc. In this work, diffraction data have been collected at pressures above the limited range of our previous study, extending the structural study of CuI-IV to the upper pressure limit of its stability. The results for data collected at $p = 3.60(2)$ GPa are listed in Table II.

The $R\bar{3}m$ structure of phase CuI-IV is illustrated in Fig. 5. The anion sublattice forms an ideal cubic close-packed anion array if the *c*/*a* ratio for the hexagonal cell has the value $2\sqrt{6} = 4.899$. However, the refined values of the cell parameters (Table II) indicate a subtle distor-

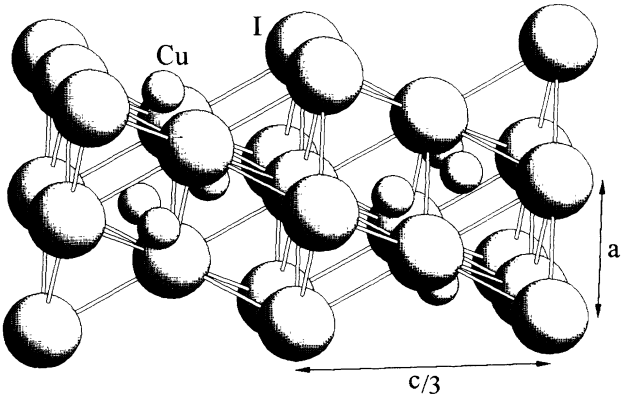

FIG. 5. The structure of the rhombohedral $R\bar{3}m$ phase of CuI-IV illustrating the location of the Cu^+ in the tetrahedral interstices of the almost regular cubic close-packed anion sublattice.

TABLE II. Results of least-squares refinements of the diffraction data for CuI. The unit-cell parameters are given and V/Z is the unit-cell volume per formula unit. The positional parameters (z_{Cu} and z_I) are given where appropriate and B_{Cu} and B_I are the isotropic thermal parameters for each species. N_d is the number of data points used in the fit, P is the number of reflections and the goodness of fit parameters R_w, R_{exp} and χ^2 are defined in Sec. II.

CuI	CuI-III $F\bar{4}3m$ $Z=4$ Cu^+ in 4a at (0,0,0) I^- in 4b at $(\frac{1}{4},\frac{1}{4},\frac{1}{4})$	CuI-IV $R\bar{3}m$ $Z=6$ Cu^+ in 6c at $(0,0,z_{Cu})$ I^- in 3a at (0,0,0) I^- in 3b at $(0,0,\frac{1}{2})$		CuI-V $P4/nmm$ $Z=2$ Cu^+ in 2a at (0,0,0) I^- in 2c at $(0,\frac{1}{2},z_I)$	
p (GPa)	Ambient	1.74(1)	3.60(2)	5.55(2)	8.39(3)
a (Å)	6.0545(3)	4.155(2)	4.0826(3)	4.0229(3)	3.9680(4)
c (Å)		20.48(1)	20.077(1)	5.6506(8)	5.5284(9)
c/a		4.929(3)	4.9176(4)	1.4046(2)	1.3932(3)
V/Z (Å^3)	55.485(5)	51.03(5)	48.300(5)	45.724(8)	43.522(9)
z_{Cu}		0.1293(4)	0.1282(2)		
z_I				0.2913(4)	0.2975(4)
B_{Cu} (Å^2)	2.86(2)	3.5(2)	2.27(3)	1.32(2)	0.94(3)
B_I (Å^2)	1.77(3)	1.5(2)	1.54(3)	0.75(4)	0.62(5)
N_d	3690	3576	4185	4186	4190
P	135	169	382	423	401
R_w (%)	1.12	6.65	2.57	2.54	3.31
R_{exp} (%)	1.10	4.13	1.77	2.04	2.55
χ^2	1.04	2.59	2.11	1.55	1.68

tion, leading to two slightly different I^--I^- distances. In addition, the cations are displaced from the center of the tetrahedral interstices within the anion sublattice, which are located at $z_{Cu}=\frac{1}{8}$. As a consequence, the regular tetrahedral coordination of Cu^+ found in zinc-blende phase III becomes distorted in CuI-IV, with one slightly longer Cu^+-I^- bond and two distinct I^--Cu^+-I^- angles spanning the ideal value of 109.47°. The $R\bar{3}m$ structure adopted by phase CuI-IV appears to be unique, though it belongs to a wider group of structures with different packing sequences along the c axis. The members of this family generally have $R\bar{3}m$ or $R3m$ symmetry and include the polytypes of CuI (Refs. 31 and 32) and several binary III-VI compounds such as InSe.[33]

Phase CuI-V

The original x-ray diffraction studies[14] identified similarities between the measured patterns from phases CuI-III, CuI-IV, and CuI-V. X-ray diffraction is dominated by scattering from the I^-, so the cubic close-packed anion sublattice present in the zinc-blende structure is probably retained through the transitions CuI-III→CuI-IV and CuI-IV→CuI-V. With this in mind, Moore, Kasper, and Bundy[14] suggested that CuI-V possesses a cubic superstructure of zinc-blende, with $a=11.463$ Å at $p=5.5$ GPa. This assignment was subsequently revised by Meisalo and Kalliomäki,[2] who successfully accounted for 11 x-ray diffraction peaks measured at $p=6.5$ GPa with a tetragonal unit cell with $a=4.02$ Å and $c=5.70$ Å. The unit cell then contains two formula units and a structure "anti" that of litharge (red-PbO) was proposed. On this assumption, band-structure calculations were found to provide a general agreement with experimental optical data.[9] Conversely, Brafman, Cardona, and Vardeny[12] were unable to reconcile their Raman data with the antilitharge configuration and conclude that the structure of CuI-V requires further investigation.

Diffraction data from pure CuI was collected at pressures of $p=5.55(2)$ GPa and $p=8.39(3)$ GPa. As shown in Table III, the observed d spacings at the lower pressure can be completely described in terms of a tetragonal cell with $a=4.02$ Å and $c=5.65$ Å. Following the work of Meisalo and Kalliomäki,[2] attempts were made to perform a least-squares fit to the experimental data at both pressures using the antilitharge structure. The I^- are placed in 2b sites at $(0,\frac{1}{2},z_I)$ and $(\frac{1}{2},0,\bar{z}_I)$ with z_I allowed by symmetry to vary away from its close-packed ideal value of $\frac{1}{4}$. The Cu^+ are located in 2a sites at (0,0,0) and $(\frac{1}{2},\frac{1}{2},0)$. The assumed structure gave excellent agreement between the measured and calculated profiles, as illustrated in Fig. 6. Therefore, the structure of CuI-V is indeed anti that of litharge, with the fitted parameters listed in Table II.

The antilitharge structure illustrated in Fig. 7 can be considered as a cubic close-packed anion sublattice swelled and distorted by the introduction of sheets of cations. The cubic close-packed anion sublattice is demonstrated by the observed tetragonal c/a ratio (1.405) being close to the expected value of $\sqrt{2}=1.414$ and the single variable coordinate $z_I\sim0.29$ being approximately $\frac{1}{4}$. The distortions of the structure are such that each I^- has four nearest-neighbor anions at each of three different distances. In this structure, the CuI_4 tetrahedra are also distorted, though the four Cu^+-I^- bonds remain equidistant and there are two different anion-cation-anion angles which are more different than the two in the rhombohedral phase.

The $P4/nmm$ structure has only two degrees of freedom but different values of c/a and the single positional

TABLE III. The measured d spacings observed at $d > 1$ Å in diffraction data collected from CuI-V at $p = 5.55(2)$ GPa. These show an excellent agreement with those expected for a tetragonal unit cell, of space group $P4/nmm$, with $a = 4.02$ and $c = 5.65$ Å. The normalized intensities for each reflection ($100 \times I/I_{max}$) are listed in the last column.

hkl	d_{calc} (Å) $a = 4.02$ Å $c = 5.65$ Å	d_{meas} (Å)	$100 \times I/I_{max}$
011	3.276	3.277(1)	63
110	2.843	2.832(5)	4
002	2.825		
111	2.539	2.540(1)	72
012	2.311	2.308(2)	6
020	2.010	2.007(3)	100
112	2.004		
021	1.894	1.888(3)	18
003	1.883		
121	1.713	1.708(3)	14
013	1.705		
022	1.638	1.636(3)	2
113	1.570	1.571(2)	3
122	1.517	1.518(2)	2
220	1.422	1.417(3)	11
004	1.413		
221	1.378	1.376(2)	17
023	1.374		
014	1.333	1.332(2)	3
031	1.304	1.301(2)	4
123	1.300		
130	1.271		
222	1.270	1.267(3)	2
114	1.265		
131	1.240	1.240(1)	9
132	1.159	1.157(2)	21
024	1.156		
223	1.134	1.133(2)	6
005	1.130		
124	1.111	1.111(2)	3
231	1.094		
033	1.092	1.089(4)	2
015	1.088		
133	1.054	1.051(2)	4
115	1.050		
040	1.005	1.003(2)	6
224	1.002		

parameter z generate structures with distinctly different coordinations. As discussed previously,[34] the (anti-) litharge structure is more densely packed than zinc blende (or its hexagonal equivalent wurtzite) if z takes a value greater than $\frac{1}{4}$ as in CuI-V. This contrasts with the litharge structured binary monoxides where, for example, red PbO has $z_{Pb} = 0.2385$. These compounds are relatively less densely packed and pressure-induced transitions from litharge *to* wurtzite may occur [as in SnO (Ref. 35)] CuI-V also shows little structural similarity to the only other antilitharge compound InBi,[36] which has $c/a = 0.954$ and $z_{Bi} = 0.393$. The double Bi layer in this

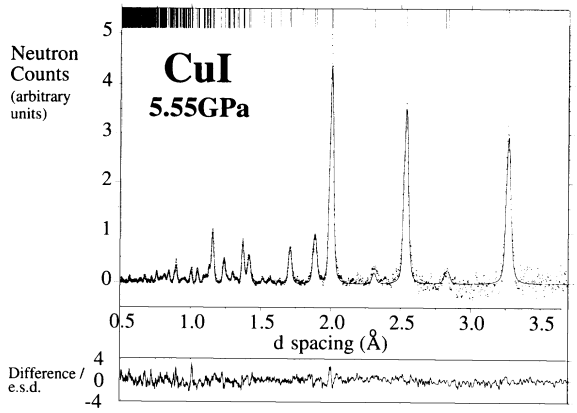

FIG. 6. Least-squares refinement of the diffraction data collected from CuI-V at $p = 5.55(2)$ GPa. The solid line is a fit to the experimental data points which are shown as dots. The lower trace shows the difference (observed-calculated) divided by the estimated standard deviation on the experimental points. The tick marks across the top mark the positions of the calculated reflections.

III-V material is less corrugated and the structure is governed by the presence of longer metallic bonds.

B. Copper (I) chloride

Table I summarizes the published information concerning the pressure-induced transitions within CuCl. The disparate values of the transition pressures can in part be attributed to uncertainties in the pressure calibration. However, CuCl is an inherently unstable compound and it is also probable that these are significantly influenced by such factors as sample purity, exposure to light and the presence of nonhydrostatic stresses within the pressure enclosure.

The quantity of published literature devoted to the high-pressure behavior of CuCl (compared to CuBr and CuI) has been motivated by reports of strong diamagnetic anomalies at $T \sim 100-170$ K and $p \sim 0.5$ GPa, taken as evidence of a Meissner effect and implying the existence

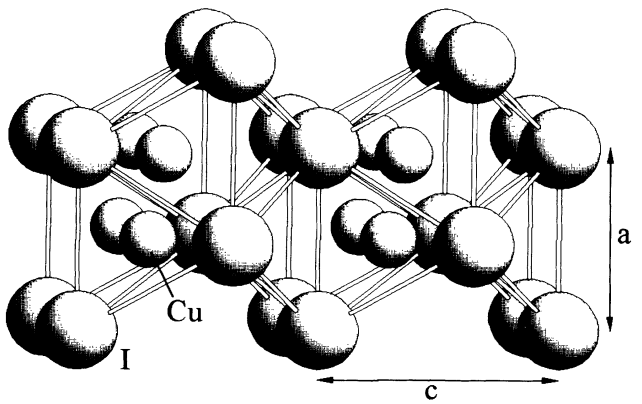

FIG. 7. The structure of the tetragonal $P4/nmm$ phase of CuI-V. In this antilitharge structure the Cu^+ are located in the tetrahedral interstices of the almost regular cubic close-packed anion sublattice.

of a superconducting state.[20] This interpretation was supported by several observations[4,21,22] of an ambient temperature metal-insulator transition at $p \sim 4$ GPa, within the stability field of the zinc-blende phase and termed CuCl-II→IIa in Table I. However, the situation is confused by reports of "irreproducibility,"[22] including apparent effects due to impurities, sample preparation, nonhydrostatic conditions[3] and the possibility of pressure-induced disproportionation ($2CuCl \rightarrow Cu + CuCl_2$).[18] The formation of free Cu could account for the opaque appearance of CuCl at $p \sim 4$ GPa (Ref. 6) and a sharp drop in resistivity at the CuCl-II→CuCl-IIa transition,[4,21] though no conclusive diffraction evidence for the disproportionation products has been reported. Such behavior might be expected because the reaction $2CuCl \rightarrow Cu + CuCl_2$ has an associated volume decrease of ~3% and should be favored at high pressure.[37] In this work, there is no diffraction evidence for either $CuCl_2$ or free Cu within phase CuCl-II or at any pressures up to 10.49(3) GPa. The sensitivity of the neutron measurements in this respect is estimated to be better than ~5% and significantly lower than the ~20% disproportionation predicted by Usha Devi and Singh.[13]

Of principal concern here are the two structural phase transitions reported in CuCl. As listed in Table I, the first transition from the zinc-blende structured phase CuCl-II to phase CuCl-IV occurs at $p \sim 5$ GPa. In this neutron-diffraction study, illustrated in Fig. 8, the first evidence of additional diffraction lines is at $p = 4.98(1)$ GPa, with an additional weak peak at $d \sim 1.72$ Å and another (not shown in Fig. 8) at $d \sim 2.64$ Å. At the next pressure, $p = 5.19(1)$ GPa, the remaining peaks from the zinc-blende phase CuCl-II are considerably reduced in intensity, indicating almost complete transformation to CuCl-IV. The transition CuCl-II→CuCl-IV therefore occurs at $p = 5.1(1)$ GPa with a maximum coexistence range of ~0.3 GPa. A further transition (CuCl-IV→CuCl-V) is said to take place at pressures somewhere in excess of ~8.0 GPa. Early reports[2,3] suggested that this transformation is rather sluggish and occurs over a wide pressure range. However, more recent measurements indicate that under hydrostatic conditions the transition is abrupt.[7] In this work, the phase transition to CuCl-V is first observed at $p = 10.29(2)$ GPa by the appearance of an additional small reflection at $d \sim 1.74$ Å. At this stage, increasing the applied load to the pressure cell produced only a small increment in measured pressure to 10.49(3) GPa. Two more peaks at $d \sim 1.42$ Å and ~2.46 Å became visible and approximately 30% of the sample was transformed from CuCl-IV to CuCl-V. Unfortunately, this pressure region is at the upper limit of the pressure cell and attempts to increase the load further (to produce single phase CuCl-V) led to failure of the tungsten carbide anvils. The transition pressure for the CuCl-IV→CuCl-V transformation is estimated to be 10.6(3) GPa.

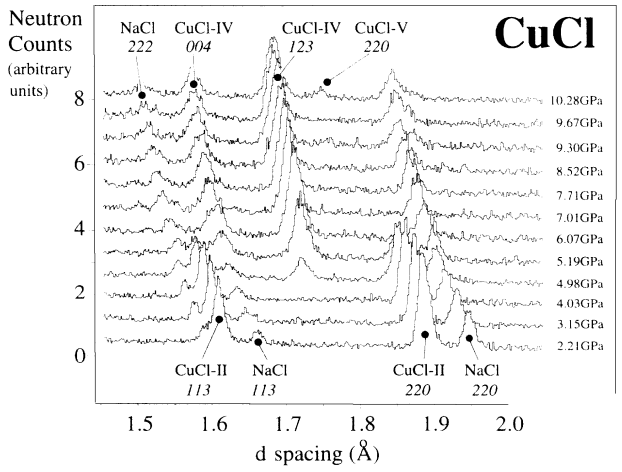

FIG. 8. Evolution of the diffraction pattern of the mixed CuCl+NaCl sample with pressure. The structural phase transitions CuCl-II→CuCl-IV and CuCl-IV→CuCl-V are observed at $p \sim 4.9$ and ~10.3 GPa, respectively.

Phase CuCl-IV

In an x-ray diffraction investigation at high pressure, Meisalo and Kalliomäki[2] observed two strong lines attributed to phase CuCl-IV with $d = 1.713$ Å and 2.618 Å at $p = 5.5$ GPa. Corresponding intense peaks are also clearly visible in the neutron-diffraction patterns collected from this phase. By including a further four weak reflections (one of which is not observed in the neutron data) these authors[2] derived a tetragonal unit cell with $a = 5.21$ Å and $c = 4.61$ Å. This assignment was subsequently revised to orthorhombic,[38] with $a = 3.586$ Å, $b = 4.550$ Å, and $c = 7.416$ Å or to a larger tetragonal unit cell[39] with $a = 6.376$ Å and $c = 6.468$ Å. A different tetragonal cell with $a = 4.89(1)$ Å and $c = 5.23(1)$ Å was determined by Serebryanaya, Popova, and Rusakov[4] also using x-ray-diffraction. Of these differing descriptions, the original one was adopted by other workers to derive the compressibility of CuCl-IV, giving volume discontinuities at the CuCl-II→CuCl-IV and CuCl-IV→CuCl-V transitions of $\Delta V/V_0 \sim 11\%$ and ~1%, respectively.[2,3,13,18] The relatively small value for the latter suggested a similarity between the structure of CuCl-IV and the rocksalt structure of CuCl-V (see below), possibly in the form of a simple tetragonal distortion.[2] A theoretical study by Smolander[40] suggested that the most likely structures for CuCl-IV are tetragonal (space group $P4_2/mcm$) with $a = 5.044$ Å and $c = 5.158$ Å or orthorhombic (space group $Fddd$) with $a = 6.980$ Å, $b = 7.607$ Å, and $c = 9.827$ Å, again using the assumption of a distortion from the rocksalt structure with the cations displaced from the centers of the anion octahedra. Raman[41] and optical absorption[9] measurements suggested that CuCl-IV has a similar structure to CuI-V, leading Blacha, Christensen, and Cardona[9] to propose that CuCl-IV has a superstructure of the antilitharge arrangement, with $a(\text{CuCl-IV}) = \sqrt{2} \times a(\text{antilitharge})$ and $c(\text{CuCl-IV}) = c(\text{antilitharge})$. However, attempts to calculate the band structure on this basis proved unsuccessful.[9]

In this work, the determination of the structure of phase CuCl-IV was made using neutron-diffraction data collected from a pure CuCl sample at $p = 5.52(2)$ GPa.

TABLE IV. The measured d spacings observed at $d > 1$ Å in diffraction data collected from CuCl-IV at $p = 5.52(2)$ GPa. These agree with those expected for a cubic unit cell, of space group $Pa\bar{3}$, with $a = 6.416$ Å. The calculated values also agree well with the x-ray diffraction observations of Meisalo and Kalliomäki (Ref. 2), with the exception of the weak peak at $d \sim 2.316$ Å which is not observed in this work and must be regarded as spurious. The normalized intensities for each reflection obtained in this work ($100 \times I/I_{max}$) are listed for comparison with those taken from the x-ray diffraction study (Ref. 2).

	d_{calc} (Å)	d_{meas} (Å)	$100 \times I/I_{max}$	d_{meas} (Å)	I
hkl	$a = 6.416$ Å	This work		Ref. 2	
111	3.704			3.66	*w*
002	3.208	3.213(3)	3		
021	2.869	2.863(4)	4	2.89	*vw*
112	2.619	2.620(1)	100	2.618	*s*
				2.316	*vw*
221	2.139	2.136(3)	5		
023	1.779	1.777(3)	2		
123	1.715	1.716(1)	66	1.713	*s*
004	1.604	1.604(2)	15	1.616	*vw*
223/041	1.556	1.556(2)	2		
114	1.512	1.511(2)	2		
331	1.472	1.473(2)	1		
042	1.435	1.435(2)	2		
332	1.368	1.368(1)	8		
224	1.310	1.308(2)	1		
134	1.258	1.257(1)	4		
333/115	1.235	1.235(1)	3		
234/025	1.191	1.192(1)	2		
125	1.171	1.173(1)	8		
044	1.134	1.135(1)	8		
441/225	1.117	1.118(2)	1		
442/006	1.069	1.070(2)	2		
061	1.055	1.055(1)	3		
235/116	1.041	1.043(1)	13		
026	1.014	1.013(3)	1		
443/045/126	1.002	1.003(2)	3		

Table IV lists the 24 observed reflections with $d > 1$ Å. In contrast to the previous determinations,[2,4,38,39] these can be completely indexed on the basis of a cubic cell with $a \sim 6.416$ Å. Of the previous structural investigations using x-ray diffraction, only the paper of Meisalo and Kalliomäki[2] includes a listing of the measured d spacings. It is clear from Table IV that this proposed cubic cell accounts adequately for their observations, with the exception of the very weak reflection at $d = 2.316$ Å which appears to be spurious. Confirmation of this assignment is provided by data collected at a pressure of $p = 9.24(2)$ GPa which could also be completely described using a cubic cell with $a \sim 6.310$ Å. The unit cell contains eight formula units and the volume discontinuities at the CuCl-II→CuCl-IV and CuCl-IV→CuCl-V transitions are more similar than suggested previously, with $\Delta V/V_0 \sim 7\%$ and $\sim 3\%$, respectively. As a consequence, suggestions that the structure of CuCl-IV is a subtle distortion of the rocksalt structure are probably invalid.

In general, the coincidence of reflections with identical values of $h^2+k^2+l^2$ in cubic symmetry makes the identification of the systematic absences difficult using powder diffraction data. However, the CuCl-IV diffraction data do indicate that there are no conditions placed on the presence of reflections of the type hkl and hhl. The former dictates that the lattice is primitive. It is also apparent that the hkl reflections which do not satisfy $h+k+l = 2n$ are systematically weak. The conditions appear to require $k = 2n$ for refections of type $0kl$ and $l = 2n$ for reflections of type $00l$. These requirements are satisfied by a single space group, $Pa\bar{3}$. However, the number of unambiguous reflections is small and the absence of the $0kl$ condition would imply the subgroup $P2_13$. Similarly, the alternative choice of $P4_132$ (or its enantiomorph $P4_332$) is only excluded by the presence of the very weak 002 reflection.

Initially both Cu^+ and Cl^- are placed in 8*c* sites of space group $Pa\bar{3}$ at (x,x,x), etc. Approximate starting values for x_{Cu} and x_{Cl} are derived by searching for a structure with physically reasonable interatomic distances, assumed to be ~ 3.5 and 2.8 Å for Cl^--Cl^- and Cu^+-Cu^+, respectively, and estimated from the neighboring phases. The length of the body diagonal of the unit cell is $\sqrt{3}a = 11.1$ Å and the chosen space group has a center of symmetry. The distance between the two atoms

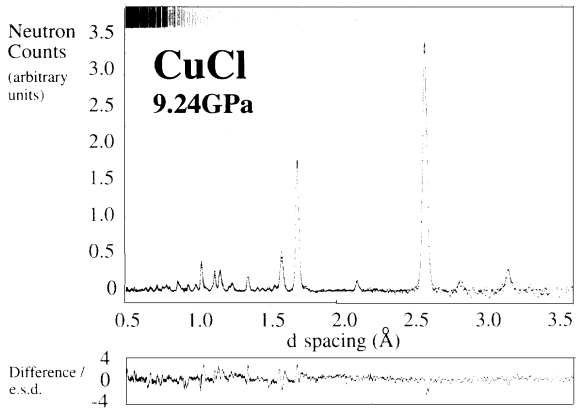

FIG. 9. Least-squares refinement of the diffraction data collected from CuCl-IV at $p=9.24(2)$ GPa. The solid line is a fit to the experimental data points which are shown as dots. The lower trace shows the difference (observed-calculated) divided by the estimated standard deviation on the experimental points. The tick marks across the top mark the positions of the calculated reflections.

at $\pm(x,x,x)$ requires $x_{Cl}=0.157$ and $x_{Cu}=0.626$. The Cu^+-Cl^- distance along the $\langle 111\rangle$ direction is then $\sqrt{3}(1-x_{Cu}-x_{Cl})a=2.4$ Å, comparable to that observed in zinc blende CuCl-II. Calculation of all the interatomic distances in the proposed structure yields no anomalously short contacts and a simulation of the expected neutron-diffraction pattern gives a good overall agreement with that measured. Least-squares refinements of the experimental diffraction profiles improved the quality of the fit further, as illustrated in Fig. 9 for the $p=9.24(2)$ GPa data. The refined values listed in Table V indicate that the two positional parameters are slightly displaced from their estimated positions.

In space group $Pa\bar{3}$ the proposed structure becomes body-centered (space group $Ia\bar{3}$) if the positional parameters satisfy the condition x_{Cu}-$x_{Cl}=\frac{1}{2}$ and if the anions and cations are identical. The first condition is almost met by the experimental values, since $x_{Cu}-x_{Cl}\sim 0.48$. In terms of the diffraction pattern, the second condition requires that the two different species have the same coherent scattering length for neutrons, b. For CuCl, $b_{Cu}=7.689\times10^{-15}$ m and $b_{Cl}=9.579\times10^{-15}$ m and the contrast is relatively modest. This simple discussion explains the weak nature of $h+k+l=2n+1$ peaks noted above and also serves as a warning on the uniqueness of the proposed structure. Attempts to refine the experimental data were made with all the possible distributions of the anions and cations within space groups $Pa\bar{3}$, $P2_13$, and $P4_132$, recalling that the latter two alternatives could not be conclusively ruled out on the basis of systematic absences of the observed reflections. However, all the other configurations give an inferior fit to the data and, in particular, do not adequately account for the intensities of the weak reflections. In addition, these alternatives can be discounted because they generate anomalously short (<3 Å) Cl^--Cl^- distances, which do not occur in the $Pa\bar{3}$ structure.

The cubic close-packed anion array is not retained in the $Pa\bar{3}$ structure of CuCl-IV, in contrast to the $R\bar{3}m$ and $P4/nmm$ structures discussed above for CuI-IV and CuI-V. The atomic arrangement is illustrated in Fig. 10. The anion sublattice approximates to the closest packing consistent with an ideal sevenfold coordination, which corresponds to $x=(\sqrt{5}-1)/8=0.1545$. The refined values of x_{Cl} (Table V) are slightly less than the optimum value, resulting in a subtle distortion with one slightly closer anion-anion contact. The Cu^+ sublattice can be considered as an interpenetrating sevenfold coordinated array, though the values of x_{Cu} are significantly smaller than the closest-packed value $x_{Cu}=(\sqrt{5}+3)/8=0.6545$. This leads to a single Cu^+-Cu^+ distance along the threefold axis which is significantly smaller than the others, as illustrated in Fig. 10. The cations are situated in the

TABLE V. Results of least-squares refinements of the diffraction data from CuCl. The positional parameters (x_{Cu} and x_{Cl}) are given where appropriate and B_{Cu} and B_{Cl} are the isotropic thermal parameters for each species. N_d is the number of data points used in the fit, P is the number of reflections and the goodness of fit parameters R_w, R_{exp} and χ^2 are defined in Sec. II.

CuCl	CuCl-II $F\bar{4}3m$ $Z=4$ Cu^+ in 4a at (0,0,0) Cl^- in 4b at $(\frac{1}{4},\frac{1}{4},\frac{1}{4})$	CuCl-IV $Pa\bar{3}$ $Z=8$ Cu^+ in 8c at (x_{Cu},x_{Cu},x_{Cu}) Cl^- in 8c at (x_{Cl},x_{Cl},x_{Cl})		CuCl-V $Fm\bar{3}m$ $Z=4$ Cu^+ in 4a at (0,0,0) Cl^- in 4b at $(\frac{1}{2},\frac{1}{2},\frac{1}{2})$
p (GPa)	Ambient	5.52(2)	9.24(2)	10.49(4)
a (Å)	5.4202(2)	6.4162(3)	6.3104(2)	4.9290(8)
V/Z (Å^3)	39.809(3)	33.017(3)	31.411(2)	29.938(8)
x_{Cu}		0.6297(3)	0.6294(3)	
x_{Cl}		0.1527(3)	0.1540(3)	
B_{Cu} (Å^2)	2.99(4)	2.11(7)	2.02(6)	1.33(6)
B_{Cl} (Å^2)	1.88(4)	1.21(5)	0.87(3)	0.77(5)
N_d	3690	3686	4190	1132
P	99	403	385	11
R_w (%)	1.14	3.98	2.05	5.54
R_{exp} (%)	1.12	3.29	1.65	5.02
χ^2	1.03	1.46	1.55	1.22

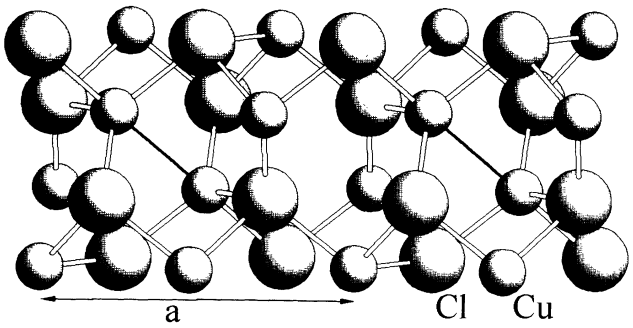

FIG. 10. The structure of the cubic $Pa\bar{3}$ phase of CuCl-IV. The approximately tetrahedral coordination of Cu^+ to four I^- is illustrated and the shorter Cu^+-Cu^+ distance is shown as a solid line.

tetrahedral cavities formed by the anion sublattice, though the tetrahedral coordination is rather heavily distorted and each $CuCl_4$ tetrahedron is linked at each vertex to three others.

The structure of phase CuCl-IV can be considered as a binary analog of the so-called BC-8 structure of Si-III (Ref. 42) and Ge-IV.[43] These are produced by quenching from the high-pressure metallic phases Si-II and Ge-II, which have the β-Sn structure. Si-III appears to be stable indefinitely while Ge-IV transforms under ambient conditions to a hexagonal form in less than one hour.[43] The quenched forms are cubic with $a=6.636(5)$ Å (Si-III) and $a=6.932(1)$ Å (Ge-IV). The atoms are located in $16c$ positions of space group $Ia\bar{3}$ at (x,x,x), etc. The single positional parameter x takes a value close to 0.1 in both phases, describing a distorted tetrahedral coordination. Alternatively, the $Pa\bar{3}$ structure can be considered as a higher symmetry counterpart to that formed by II-V compounds such as ZnAs,[44] ZnSb,[45] CdAs,[44] and CdSb.[45] These are essentially intermetallic and crystallize in the orthorhombic subgroup *Pbca* with a considerably more irregular tetrahedral environment.

Phase CuCl-V

As discussed above, only limited transformation from CuCl-IV to CuCl-V was possible at the maximum pressure. The additional peaks observed at $d\sim1.42$, ~1.74, and ~2.46 Å correspond to the 222, 220, and 200 reflections from a rocksalt structure with $a\sim4.92$ Å. Least-squares refinements of the data collected from the mixed-phase sample indicate that CuCl-V has $a=4.9290(8)$ Å, at $p=10.49(2)$ GPa. This is consistent with the values reported previously, $a=4.90$ Å at $p=12.3(2)$ GPa (Ref. 3) and $a=4.898(7)$ Å at $p=12.0$ GPa.[4] However, previous workers observed the rocksalt structured phase at lower pressures, with $a=4.931$ Å at $p=7.0$ (Ref. 2) and $a=4.96$ Å at $p=8.2(2)$ GPa.[3]

C. Copper (I) bromide

The p-T phase diagram of CuBr (Fig. 2) is less well determined than those of CuI and CuCl though it shows a general similarity to the latter (Fig. 1). However, the evolution of the diffraction pattern of CuBr with pressure (Fig. 11) is considerably more complicated, with three

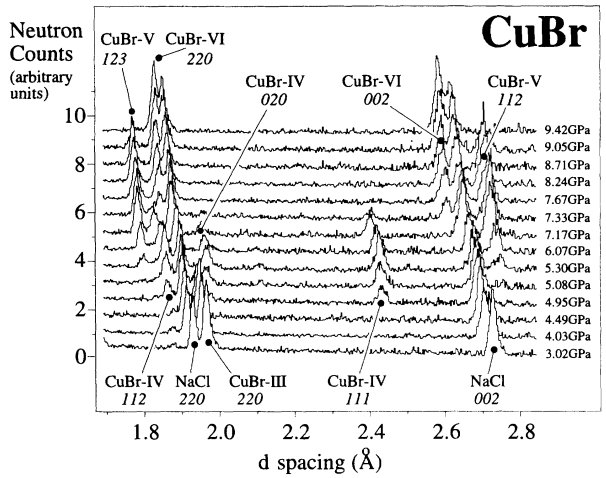

FIG. 11. Evolution of the diffraction pattern of the mixed CuBr+NaCl sample with pressure. The sluggish transitions between the four phases CuBr-III, CuBr-IV, CuBr-V, and CuBr-VI over the pressure range from ~4.9 to ~9.3 GPa are illustrated.

structural transformations occurring over wide pressure ranges and widespread coexistence of neighboring phases.

Evidence for one, or possibly two, transitions in the region $p\sim5$ GPa was provided by the optical measurements of Edwards and Drickamer[5] and van Valkenburg.[6] The stability region of CuBr-IV appeared very narrow, perhaps only ~0.5 GPa wide. In the most recent experimental study using the EXAFS technique, Tranquada and Ingalls[11] conclude that phase CuBr-IV does not exist and may arise from "transient disproportionation" (i.e., 2 CuBr-III$\rightarrow$Cu+$CuBr_2\rightarrow$2CuBr-V). There is little agreement within the published literature for the pressure at which the next transition, CuBr-V$\rightarrow$CuBr-VI, occurs. The most likely explanation is that the transformation is rather sluggish,[2] requiring a nucleation and growth mechanism, with a wide mixed-phase region.[11] The situation is further confused by conflicting evidence for[19] and against[11] pressure-induced disproportionation in CuBr at pressures in the region of ~7 GPa.

At $p\sim4.8$ GPa new diffraction lines are observed, such as those at $d\sim1.86$, ~1.96, and ~2.43 Å in Fig. 11. These increase in intensity at the expense of those from zinc blende CuBr-III until the latter disappear at $p\sim5.2$ GPa. At $p\sim5.0$ GPa a third phase, characterized by reflections at $d\sim1.79$ and ~2.74 Å, also appears. With reference to the p-T phase diagram (Fig. 2), the first new phase can be identified as the elusive CuBr-IV and the second is CuBr-V. The proportion of CuBr-V increases up to ~7.2 GPa, at the expense of CuBr-IV which is not observed at $p>7.4$ GPa. At this pressure another set of diffraction lines are observed at $d\sim1.84$ and ~2.61 Å (Fig. 11) which grow in intensity up to $p\sim9.3$ GPa. At this pressure no remaining lines from CuBr-V can be seen and the sample is single phase CuBr-VI.

Phase CuBr-IV

It is clear from Fig. 11 that phase CuBr-IV does exist, though always in the presence of one, or both, of the

TABLE VI. Results of least-squares refinements of the diffraction data from CuBr. In mixed-phase pressure regions the volume fraction of each phase is listed. The positional parameters (z_{Cu}, x_{Cu}, and x_{Br}) are given where appropriate and B_{Cu} and B_{Br} are the isotropic thermal parameters for each species. N_d is the number of data points used in the fit, P is the number of reflections and the goodness of fit parameters R_w, R_{exp}, and χ^2 are defined in Sec. II.

CuBr	CuBr-III $F\bar{4}3m$ $Z=4$ Cu^+ in 4a at (0,0,0) Br^- in 4b at $(\frac{1}{4},\frac{1}{4},\frac{1}{4})$		CuBr-IV $P4/nmm$ $Z=2$ Cu^+ in 2a at (0,0,0) Br^- in 2c at $(0,\frac{1}{2},z_{Br})$		CuBr-V $Pa\bar{3}$ $Z=8$ Cu^+ in 8c at $(x_{Cu},x_{rman}Cu,x_{Cu})$ Br^- in 8c at (x_{Br},x_{Br},x_{Br})		CuBr-VI $Fm\bar{3}m$ $Z=4$ Cu^+ in 4a at (0,0,0) Br^- in 4b at $(\frac{1}{2},\frac{1}{2},\frac{1}{2})$
p (GPa)	Ambient	4.85(2)			5.08(2)	7.29(2)	9.28(3)
Volume (%)	100	54(1)	43(1)	55(1)	45(1)	69(1)	100
a (Å)	5.6955(2)	5.4980(2)	3.9411(2)	3.9397(2)	6.7378(2)	6.6674(1)	5.1701(6)
c (Å)			5.0054(4)	5.0033(6)			
c/a			1.2701(1)	1.2700(2)			
V/Z (Å^3)	46.189(3)	41.548(3)	38.873(4)	38.829(5)	38.235(2)	37.049(1)	34.549(7)
z_{Br}			0.2931(5)	0.2927(7)			
x_{Cu}					0.6291(4)	0.6289(2)	
x_{Br}					0.1525(5)	0.1536(2)	
B_{Cu} (Å^2)	2.91(4)	2.88(4)	2.61(7)	2.78(8)	2.33(5)	2.20(4)	1.33(6)
B_{Br} (Å^2)	1.70(3)	1.55(3)	1.01(4)	1.05(6)	1.13(4)	0.92(3)	0.77(5)
N_d	3695	3524			3952	3792	3690
P	118	100	359	355	465	455	55
R_w (%)	1.20	2.84			3.48	2.85	5.79
R_{exp} (%)	1.15	2.28			2.72	2.27	5.24
χ^2	1.08	1.55			1.64	1.58	1.22

neighboring phases. Previous x-ray-diffraction studies[2,19] have failed to observe any diffraction lines attributable to CuBr-IV and the only structural information is provided by the strong optical birefringence indicating a noncubic basis.[2,6]

Simulations of the diffraction pattern of CuBr-IV were made using the structures of the high-pressure phases determined previously ($R\bar{3}m$, $P4/nmm$, and $Pa\bar{3}$). The unit cell parameter(s) were chosen to give a volume per formula unit V/Z of 40 Å^3, estimated from the corresponding value for zinc-blende CuBr-III material in the two-phase mixture. The measured neutron-diffraction data for CuBr-IV showed some similarities to that calculated using the antilitharge structure of CuI-V, though a number of single diffraction peaks in the latter appeared as separated doublets in the experimental pattern. Trials of the possible distortions of the antilitharge structure indicated that CuBr-IV possesses the same space group ($P4/nmm$) but the anion sublattice is significantly distorted away from cubic close packing with $a \sim 3.94$ Å and $c \sim 5.01$ Å, giving $c/a \sim 1.27$. The apparent difference between the diffraction patterns of the two antilitharge phases CuBr-IV and CuI-V results from the latter having a c/a ratio close to $\sqrt{2}$, resulting in the overlap of reflections such as 110 and 002 which are separated in CuBr-IV. Refinements of the data collected from the mixed-phase CuBr-III+CuBr-IV sample at $p=4.85(2)$ GPa provided an excellent fit to the data (Fig. 12 and Table VI). A similar quality fit to mixed-phase CuBr-IV+CuBr-V data collected at $p=5.08(2)$ GPa (following the determination of the structure of CuBr-V described below) confirmed that CuBr-IV has the antilitharge structure.

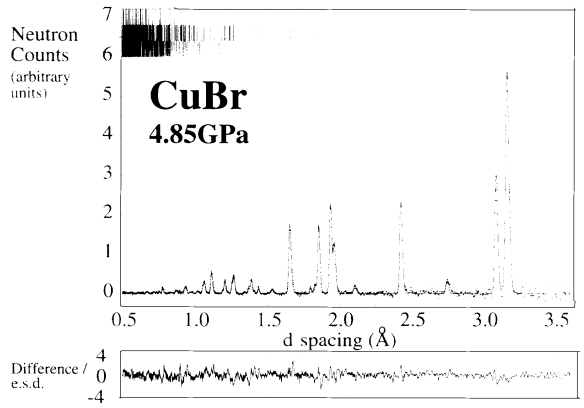

FIG. 12. Least-squares refinement of the diffraction data collected from mixed phase CuBr-III+CuBr-IV+CuBr-V at $p=4.85(2)$ GPa. The solid line is a fit to the experimental data points which are shown as dots. The lower trace shows the difference (observed-calculated) divided by the estimated standard deviation on the experimental points. The tick marks across the top mark the positions of the calculated reflections for phase CuBr-III (upper row), CuBr-IV (middle row) and CuBr-V (lower row).

Phase CuBr-V

Figure 11 illustrates that CuBr exists as a two, or sometimes three, phase mixture in the pressure range from 4.8 to 9.3 GPa. As a consequence, there is little value in providing more than a summary of the previous attempts to determine the structure of phase CuBr-V which assume it is single phase. On the basis of optical absorption measurements,[6] CuBr-V was originally suggested to be cubic. The x-ray diffraction studies of

Meisalo and Kalliomäki[2] observed two strong diffraction lines and a further three weak ones at $p=5.5$ GPa. The strong resemblance to the diffraction pattern of CuCl-IV was noted and a tetragonal unit cell with $a=5.40$ Å and $c=4.75$ Å was chosen. Although not explicitly stated, these authors presumably discounted the simpler cubic indexing because the sample appeared to be weakly birefringent. However, this optical feature could result from some remaining phase CuBr-IV. Despite similarities between the Raman spectra for CuBr-V and CuI-V,[41] the antilitharge structure was shown to be inconsistent with EXAFS data collected at $p\sim5$ GPa.[11] The latter workers also discounted the possibility of a simple tetragonal or orthorhombic distortion of the zinc-blende structure but were unable to provide a structural model consistent with their experimental data.

Investigation of the structure of phase CuBr-V used data collected at $p=7.29(2)$ GPa. This pressure is close to the highest pressure before diffraction lines from phase CuBr-VI appear. This gives the maximum phase fraction of CuBr-V, with approximately 30% of the sample still in phase CuBr-IV. The similarity between the diffraction patterns of CuBr-V and CuCl-IV noted in previous x-ray work[2] is also clear with neutron diffraction (compare Figs. 13 and 10). The observed d spacings can be successfully indexed on the basis of a primitive cubic cell with $a\sim6.75$ Å and the observed reflections are consistent with $Pa\bar{3}$ symmetry. Refinements of the diffraction data using the structure determined above for phase CuCl-IV give an excellent fit to the experimental data (Fig. 13) and good values for the quality of fit parameter χ^2 (Table VI). The fitted positional parameters x_{Cu} and x_{Br} are close to the corresponding values for phase CuCl-IV (Table V).

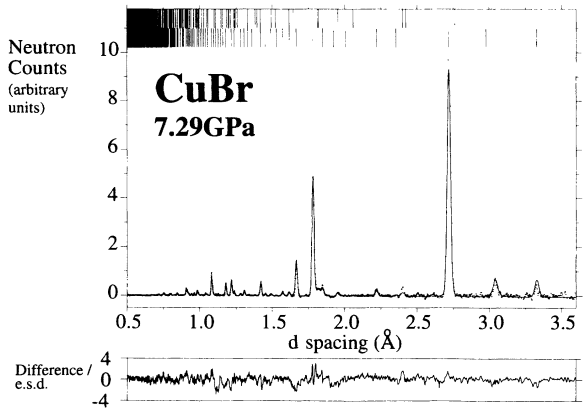

FIG. 13. Least-squares refinement of the diffraction data collected from mixed phase CuBr-IV+CuBr-V at $p=7.29(2)$ GPa. The solid line is a fit to the experimental data points which are shown as dots. The lower trace shows the difference (observed-calculated) divided by the estimated standard deviation on the experimental points. The tick marks across the top mark the positions of the calculated reflections for phase CuBr-IV (upper row) and CuBr-V (lower row).

Phase CuBr-VI

In common with phase CuBr-V, little reliable structural information can be derived from the published literature for CuBr-VI in the pressure range 6–10 GPa. The optical-absorption measurements[6] suggested two transitions, from cubic→noncubic at $p\sim8.0$ GPa and back to cubic at $p\sim9.5$ GPa. It is likely that the noncubic region in fact represents the pressure range with a significant mixture of phases CuBr-V and CuBr-VI. Meisalo and Kalliomäki[2] observed a sluggish transition at $p=6.6$ GPa to a colorless phase identified as CuBr-VI which, on the basis of six x-ray diffraction lines, possesses the rocksalt structure with $a=5.14$ Å at $p=7.5$ GPa. Energy dispersive x-ray diffraction studies by Skelton *et al.*[19] subsequently provided evidence for pressure-induced disproportionation in CuBr with the observation of $CuBr_2$ (but not free Cu) in samples at ambient conditions after pressurizing to 7 GPa. However, the EXAFS study of Tranquada and Ingalls[11] gave no evidence for disproportionation, either in samples recovered from $p=7.4$ GPa or studied *in situ*. In common with CuCl, there is no evidence using neutron diffraction for pressure-induced disproportionation within CuBr at any pressure.

On increasing pressure, the first evidence for the appearance of phase CuBr-VI is two additional weak peaks at $d\sim2.605$ and $d\sim1.842$ Å in data collected at $p=7.32(2)$ GPa. These were initially assigned to the 002 and 220 reflections from a cubic phase with $a=5.21$ Å. At the maximum pressure no remaining lines from phase CuBr-V are observed. The diffraction pattern then comprises of the NaCl pattern with a second one arising from CuBr-VI, displaced slightly to lower d spacings. The almost identical distribution of intensities clearly indicates that CuBr-VI has the rocksalt structure, confirmed by least-squares refinements of the data from pure CuBr-VI collected at $p=9.28(3)$ GPa (Fig. 14 and Table VI).

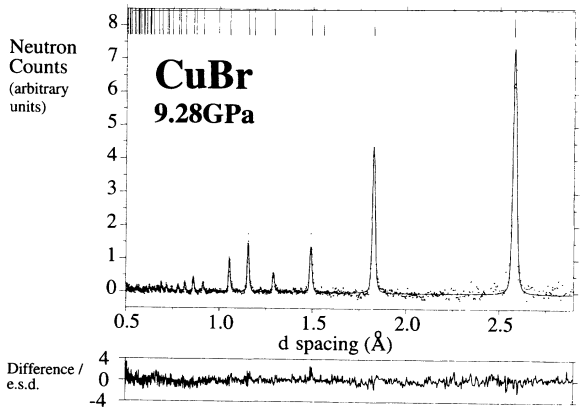

FIG. 14. Least-squares refinement of the diffraction data collected from single phase CuBr-VI at $p=9.28(3)$ GPa confirming the rocksalt structure. The solid line is a fit to the experimental data points which are shown as dots. The lower trace shows the difference (observed-calculated) divided by the estimated standard deviation on the experimental points. The tick marks across the top mark the positions of the calculated reflections.

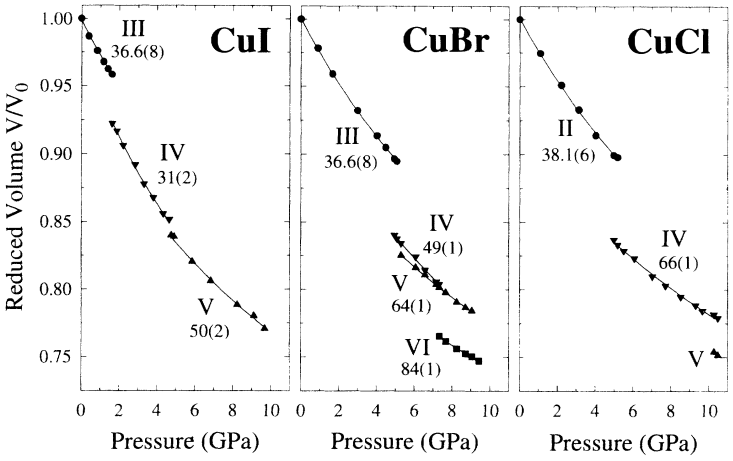

FIG. 15. The compressibility of the three Cu(I) halides plotted as reduced volume (V/V_0) versus pressure. The symbols denote the various phase as follows; ● for CuI-III, CuBr-III, and CuCl-II; ▼ for CuI-IV, CuBr-IV, and CuCl-IV; ▲ for CuI-V, CuBr-V, and CuCl-V and ■ for CuBr-VI. The errors on the plotted points are comparable with the size of the symbols. The values next to each curve give the bulk modulus of each phase in units of GPa.

IV. DISCUSSION

The equation of state for each Cu(I) halide is illustrated in Fig. 15 in the form of reduced volume V/V_0 versus pressure p. The isothermal bulk moduli (B_0) are included in Fig. 15 and are determined by fitting the Birch equation[46]

$$p=\frac{3}{2}B_0\left[\left[\frac{V_0}{V}\right]^{7/3}-\left[\frac{V_0}{V}\right]^{5/3}\right]\times\left\{1-\frac{3}{4}(4-B_0')\left[\left[\frac{V_0}{V}\right]^{2/3}-1\right]\right\} \quad (4)$$

to the experimental data for V/V_0. In practice, attempts to vary the first pressure derivative of the bulk modulus (B_0') away from its nominal value of 4.0 did not yield significant improvement to the quality of the fit. This is a consequence of the limited pressure range over which a given phase exists. The values of B_0 given in Fig. 15 are all derived for $B_0'=4.0$. The bulk moduli of the three zinc-blende phases are in good agreement with those previously measured[13,15,47–49] and calculated.[50] The rhombohedral phase of CuI-IV appears anomalous, being considerably more compressible than CuI-III and CuI-V. The bulk moduli of phases CuBr-IV and CuBr-V show the expected similarities with the values for the isostructural phases CuI-V and CuCl-IV, respectively. The appearance of phase CuBr-VI at relatively low pressures allows an estimate of $B_0=84(1)$ GPa for the rocksalt structure.

The fitted values of B_0 are used in Eq. (4) to determine the volume change at each transition, $\Delta V/V_0$, listed in Table I. The transition CuI-IV→CuI-V involves a relatively small volume collapse, in agreement with the 1% value obtained using the x-ray diffraction technique.[2] However, the volume changes at the transitions CuCl-II→CuCl-IV and CuCl-IV→CuCl-V differ considerably from those reported previously,[2–4,13,18] because the earlier work is based on fallacious tetragonal assignments for the unit cell of CuCl-IV. On the basis of the published data for phase CuI-VIII,[2] a value of $\Delta V/V_0\sim 17\%$ is estimated for the transformation to octahedral coordination in the rocksalt structure. However, as discussed below, the experimental data for phase CuI-VIII cannot be considered reliable. In the absence of abrupt transitions in CuBr, the volume differences between the various phases are calculated at pressures close to the lowest pressure at which the new phase is observed. These values are $p=4.95$ GPa (CuBr-III→CuBr-IV), $p=5.30$ GPa (CuBr-IV→CuBr-V), and $p=7.33$ GPa (CuBr-V→CuBr-VI).

The evolution of the structure of each compound over the pressure range 0–10 GPa is discussed in the following subsections. The pressure variation of the bond lengths and interbond angles is illustrated in Figs. 16–19. The high-pressure structural properties of the Cu(I) halides are then compared with the other tetrahedrally coordinated I-VII compound AgI and with the II-VI and III-V semiconductors.

A. Copper (I) iodide

On the basis of the work presented here, the pressure-induced phase transitions in CuI are zinc blende($F\bar{4}3m$)→rhombohedral($R\bar{3}m$) → antilitharge($P4/nmm$). In this work we cannot explicitly rule out the possibility of another phase between antilitharge and rocksalt ($Fm\bar{3}m$). The experimental data to assess the rocksalt structure of phase CuI-VIII is limited to a single x-ray-diffraction study at $p=12.0$ GPa.[2] This measurement was made at ambient temperature after the sample had been heated to enhance the kinetics of the transformation. Only four reflections were observed, of which three are consistent with a rocksalt structure with $a=5.15$ Å. The relatively small value of lattice parameter (compared to the rocksalt phase of CuBr) is also rather surprising. Unfortunately, the present apparatus does not allow measurements to be made at pressures significantly in excess of ~10 GPa.

The crystal structures of phases CuI-III, CuI-IV, and CuI-V can all be derived from an ideal cubic close-packed anion sublattice, in which the cations are located in perfect tetrahedral coordination. There are two tetrahedral interstices for every one Cu^+ and the cations are distributed in different ways over these sites in each phase.

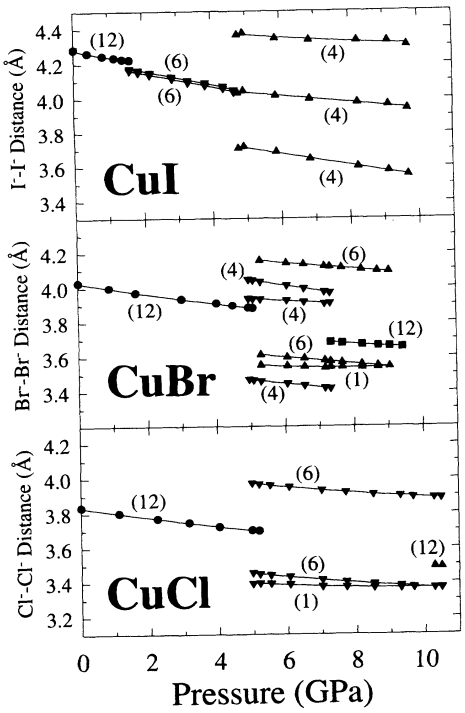

FIG. 16. The pressure variation of the anion-anion distances for the three Cu(I) halides. The values in parentheses give the number of equivalent contacts at that distance. The symbols denote the various phases as follows; ● for CuI-III, CuBr-III, and CuCl-II; ▼ for CuI-IV, CuBr-IV, and CuCl-IV; ▲ for CuI-V, CuBr-V, and CuCl-V, and ■ for CuBr-VI. The errors on the plotted points are comparable with the size of the symbols.

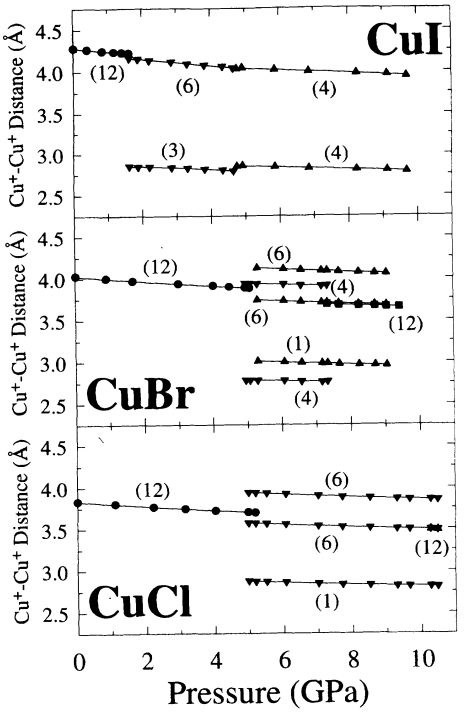

FIG. 17. Pressure variation of the cation-cation distances for the three Cu(I) halides. The values in parentheses give the number of equivalent contacts at that distance. The symbols denote the various phases as follows; ● for CuI-III, CuBr-III, and CuCl-II; ▼ for CuI-IV, CuBr-IV, and CuCl-IV; ▲ for CuI-V, CuBr-V, and CuCl-V and ■ for CuBr-VI. The errors on the plotted points are comparable with the size of the symbols.

For the idealized structures, Fig. 20 illustrates the different packings of the CuI_4 tetrahedra, which share four vertices in CuI-III, one vertex and three edges in CuI-IV and four edges in CuI-V. Such a redistribution of the cations within an ideal cubic close-packed lattice generates three structures with identical packing densities. Clearly, the distortions from these ideal topologies are important for an understanding of the mechanism of the reduction of volume with increasing pressure.

The cubic close-packed anion sublattice of the zinc-blende structured phase CuI-III undergoes a slight distortion in the rhombohedral phase CuI-IV, with two sets of six I^--I^- distances which differ by only $\sim 0.3\%$. The distortion does not change significantly with pressure and causes the tetrahedral voids to become slightly irregular, though all remain identical. The tetrahedral coordination has a single longer Cu^+-I^- bond and two sets of three I^--Cu^+-I^- angles which span the ideal value of 109.47°. The principal change at the CuI-III→CuI-IV transition is the appearance of shorter Cu^+-Cu^+ distances (~ 2.8 Å), resulting from the change to edge sharing of the CuI_4 tetrahedra. Such distances are not anomalous, though it is not clear why this structure should be favored over a simple rhombohedral distortion of the corner sharing zinc-blende structure (space group $R3c$). In phase CuI-V there is a more significant distortion of the anion sublattice with three different I^--I^- distances. The structure of CuI-V is also characterized by a distorted tetrahedral coordination of Cu^+ but with an increased number of shorter Cu^+-Cu^+ distances associated with the edge sharing CuI_4 tetrahedra. With increasing pressure, both the c/a ratio and the value z_I move further from their ideal values and the degree of distortion to both anion and cation environments increases. Finally, it is interesting to note that the preference for tetrahedral coordination of Cu^+ in the high-pressure phases CuI-IV and CuI-V is mirrored in the high-temperature phases. Extensive thermally induced disorder involves the dynamic redistribution of the cations over the available tetrahedral interstices within hexagonal close-packed (CuI-II)[51] and cubic close-packed (CuI-I)[52] anion sublattices.

B. Copper (I) chloride

The zinc-blende($F\bar{4}3m$)→cubic($Pa\bar{3}$)→rock-salt($Fm\bar{3}m$) sequence of transitions in CuCl does not retain the cubic close-packed Cl^- sublattice, even in a distorted form. In CuCl-IV the first coordination shell has six equal Cl^--Cl^- distances and one slightly shorter contact. As illustrated in Fig. 16, these become more equal with increasing pressure. The second coordination shell has a further six Cl^- at a distance ~ 3.9 Å. Through the CuCl-II→CuCl-IV→CuCl-V transitions the anion-anion

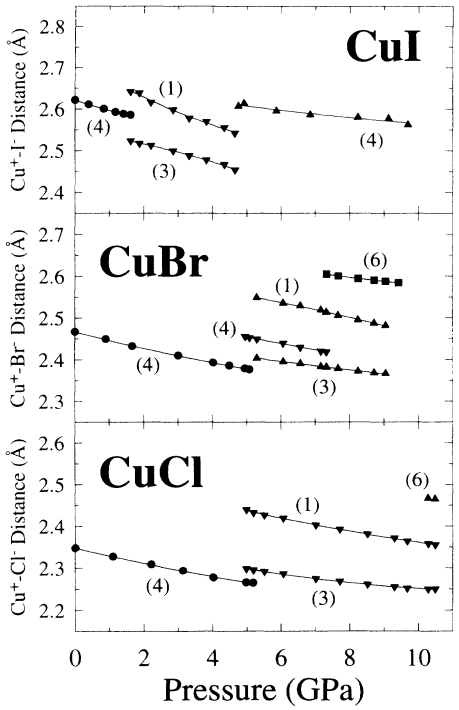

FIG. 18. Pressure variation of the anion-cation distances for the three Cu(I) halides. The values in parentheses give the number of equivalent contacts at that distance. The symbols denote the various phases as follows; ● for CuI-III, CuBr-III, and CuCl-II; ▼ for CuI-IV, CuBr-IV, and CuCl-IV; ▲ for CuI-V, CuBr-V, and CuCl-V, and ■ for CuBr-VI. The errors on the plotted points are comparable with the size of the symbols.

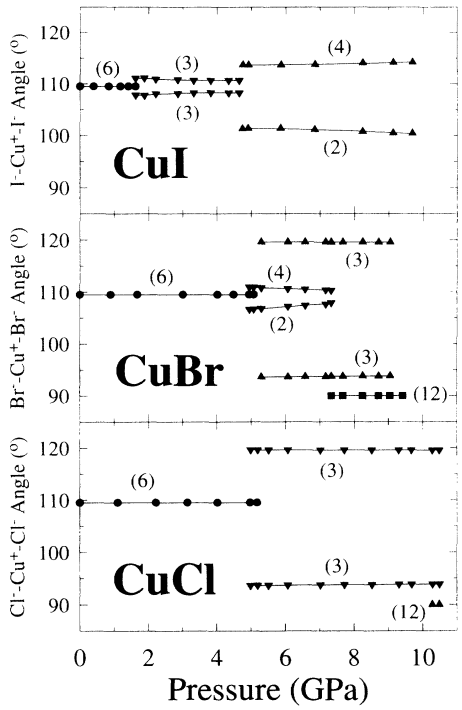

FIG. 19. Pressure variation of the anion-cation-anion angles for the three Cu(I) halides. The values in parentheses give the number of equivalent angles with the same value. The symbols denote the various phases as follows; ● for CuI-III, CuBr-III, and CuCl-II; ▼ for CuI-IV, CuBr-IV, and CuCl-IV; ▲ for CuI-V, CuBr-V, and CuCl-V, and ■ for CuBr-VI. The errors on the plotted points are comparable with the size of the symbols.

coordination changes from a regular twelvefold coordination to one with essentially (7+6) coordination and then reverts back to the ideal twelvefold coordinated array. In terms of the Cu^+-Cu^+ distances, the intermediate CuCl-IV phase has essentially 13 cations in the first coordination shell, of which one is considerably closer than the rest. However, this distance is still larger than that estimated if CuCl adopted the rhombohedral or antilitharge structures of CuI-IV and CuI-V. The difference between the pressure-induced transitions in CuI and CuCl is consistent with the smaller cation centered tetrahedra in the latter. Edge sharing of the polyhedra would result in cation-cation contacts less than ~2.5 Å in CuCl, which may be less energetically favorable. Instead the tetrahedral Cu^+ coordination to four anions is rather more distorted in CuCl than in CuI, particularly in terms of the interbond angles (Fig. 19). This presumably is a consequence of the less covalent nature of the bonds in CuCl and the difficulty in accommodating the Cu^+ in the smaller tetrahedral interstices in the Cl^- sublattice.

C. Copper (I) bromide

The refined value of the anion positional parameter z_{Br} in CuBr-IV is very close to the corresponding value in the isostructural CuI-V. However, the lower value of c/a in the former gives rise to a markedly different Br^--Br^- coordination, with four neighbors at ~3.5 Å and the remaining 8 at ~4.0 Å. The anion sublattice in the antilitharge structure is comprised of layers of square planar coordinated anions, the distance between atoms in the plane being a. These layers are perpendicular to the c axis with tetrahedral interstices between them. The Cu^+

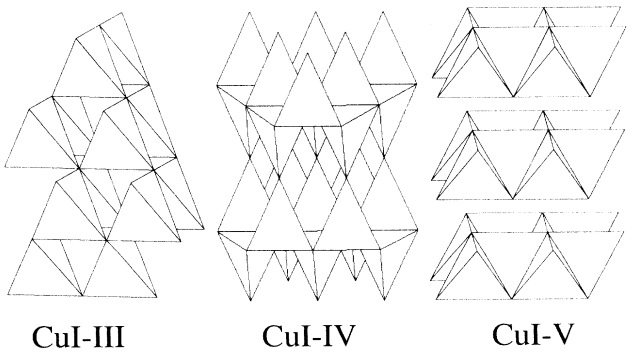

FIG. 20. Schematic diagram showing the different arrangements of the CuI_4 tetrahedral units in CuI. On increasing pressure, the tetrahedra share four vertices (zinc blende, CuI-III) then one vertex and three edges (rhombohedral, CuI-IV) and finally four edges (anti-litharge, CuI-V). At higher pressures it is expected that CuI adopts the octahedrally coordinated rock-salt structure.

form square-planar sheets with a Cu^+-Cu^+ distance $a/\sqrt{2}$ which occupy all the tetrahedral interstices within alternate layers. This has the effect of swelling the gap between the anion layers, which becomes larger than the gap with unfilled tetrahedral cavities. The extent of the distortion of the anion sublattice is significantly larger in CuBr than in CuI. Furthermore, the difference between the three different anion-anion distances increases with pressure in CuBr (Fig. 16). The relatively small volume difference between CuBr-IV and CuBr-V and the wide pressure range over which they coexist suggests that the two structures differ little in their energies. The structural trends within phase CuBr-V mirror those discussed above for the isostructural CuCl-IV, particularly with regard to the increasing similarity of the seven nearest-neighbor anion-anion contacts.

D. Other zinc-blende structured compounds

The obvious comparison of the high-pressure structural properties of the Cu(I) halides is with the Ag halides. Of these, AgCl and AgBr can be discounted because they adopt the rocksalt structure under ambient conditions. AgI usually exists as a mixture of wurtzite (AgI-II) and zinc blende (AgI-II'), of which the former is believed to be the more stable.[53] Previous neutron-diffraction results on decreasing pressure show that the rocksalt phase AgI-III transforms to pure AgI-II' via an intermediate phase AgI-IV,[34] which is stable between ~ 0.38 and ~ 0.27 GPa.[54] The AgI-III$\rightarrow$AgI-IV transformation is very sluggish and requires over 2 days to complete. AgI-IV possesses the antilitharge structure,[34] though in a more distorted form than CuI-V and similar to that of CuBr-IV. Despite the difference in pressure scales and the apparent absence of a rhombohedral $R\bar{3}m$ phase in AgI, there is a clear relation to the behavior of CuI. This conflicts with the work of Hinze,[30] who concludes that marked differences exist in their high-pressure behavior due to the additional $4d$ shell in Ag and the resulting increase in screening of the valence electrons.

The influence of hydrostatic pressure on the structural and electronic behavior of the tetrahedrally coordinated III-V and II-VI compounds has long been a popular topic in condensed-matter research. In their 1966 review, Klement and Jayaraman[17] conclude that the fourfold coordinated zinc-blende (or the related wurtzite) structure of the III-V and II-V compounds collapses to an ordered β-Sn phase, with (4+2) coordination, if the electronegativity difference between the constituent elements is relatively small. For larger differences, the first transition is to the octahedrally coordinated rocksalt structure or, in the case of the Hg compounds, to a cinnabar phase with a more distorted (4+2) environment. Although recent measurements have identified some exceptions,[55–57] this general description remains valid today.

The high-pressure trends observed in the I-VII compounds bear little resemblance to those of the more covalently bonded semiconductors, though the incomplete structural information for the latter does not permit conclusive statements to be made. With the possible exception of InBi discussed above, the three intermediate structures observed in the Cu(I) halides do not occur in any of the II-VI or III-V compounds, at either ambient or elevated pressures. These structures retain the fourfold coordination, albeit in a distorted form, and there is no tendency towards the (4+2) coordination observed in several high-temperature phases of III-V and II-VI compounds.[17] The $R\bar{3}m$ and $P4/nmm$ structures adopted by CuI on increasing pressure have a next-nearest neighbor anion distance of $> \sim 4.7$ Å from the Cu^+, while in the $Pa\bar{3}$ structure the second coordination shell is at ~ 3.5 Å. This preference for tetrahedral coordination in the Cu(I) halides appears counter intuitive because the bonding is more ionic in character. As such, it is more appropriate to consider steric constraints and the fourfold coordination stems from the ability of the relatively small Cu^+ to reside in the tetrahedral interstices in the anion sublattice. The difference in "ionic" sizes is greatest in CuI and the Cu^+ can be accommodated in the cubic close-packed anion array with relatively minor distortions. In CuCl, the two species are more comparable in size. The tetrahedral coordination in the intermediate CuCl-IV phase is more distorted and the cation sublattice also tends towards a close-packed array.

Finally, it should be noted that considerable theoretical effort has been applied to predict the high-pressure behavior of the tetrahedrally coordinated compounds,[58,59] because it provides a valuable test of various models for the interatomic bonds. While there has been some success with the group IV elements and the III-IV and II-VI semiconductors, the I-VII compounds have proved more problematic and the calculations are complicated by the strong interaction between the Cu $3d$ band and the halide p bands.[59] It is hoped that the structural information provided in this paper will motivate more theoretical studies of the I-VII systems.

V. SUMMARY AND CONCLUSIONS

The structural properties of the Cu(I) halides have been investigated at pressures up to ~ 10 GPa using powder diffraction at a pulsed neutron source. With this technique, the fixed scattering geometry (with $2\theta \sim 90°$) allows diffraction data to be collected over a wide d-spacing range with essentially constant resolution and without contamination of the pattern by spurious peaks from the pressure cell components. As a consequence, the structures of the high-pressure phases have been unambiguously determined, resolving several long running controversies and correcting a number of errors in the published literature.

The expected change from the fourfold coordinated zinc-blende structure to the sixfold coordinated rocksalt structure is confirmed in both CuCl and CuBr. No such transformation is observed in CuI up to 9.69 GPa, presumably because it occurs at a pressure above this maximum. The transformation from tetrahedral to octahedral coordination occurs via a single intermediate phase (IV) in CuCl, stable between 5.1(a) and 10.6(3) GPa. In CuI there are (at least) two intermediate phases, the abrupt transitions to phases CuI-IV and CuI-V are observed at $p = 1.63(1)$ GPa and $p = 4.70(5)$ GPa, respectively. CuBr behaves rather differently, the transition from zinc blende to rocksalt occurs via two inter-

mediate phases (CuBr-IV and CuBr-V) but the transformations occur over wide pressure ranges. In particular, the diffraction data clearly show that the elusive phase CuBr-IV exists, though always in the presence of one, or both, of the neighboring phases. Pressure-induced disproportionation is not observed in any of the compounds. It seems likely that this process only occurs under severely nonhydrostatic conditions.

The crystal structures of the intermediate phases have space groups $R\bar{3}m$ (CuI-IV), $P4/nmm$ (CuI-V and CuBr-IV) and $Pa\bar{3}$ (CuCl-IV and CuBr-V). All three can be considered as more densely packed structures which retain the tetrahedral cation coordination. The tetrahedral coordination is more regular in CuI and the sequence of structural transitions can be considered as a transformation from corner to edge sharing CuI_4 tetrahedra. The cubic close-packed anion sublattice appears to be retained through the transitions, though with a slight distortion in CuI-IV and a more significant departure from twelvefold coordination in CuI-V. The fourfold cation-anion coordination is rather distorted in CuCl-IV, though the $CuCl_4$ units continue to share corners. This structure can be considered as an ordered binary counterpart to that adopted by Si and Ge following decompression from high pressure. In conclusion, the increase in packing density is accommodated by shorter Cu^+-Cu^+ distances. The intermediate phases observed in the Cu(I) halides between the zinc blende and rocksalt structured phases show no tendency towards an octahedral environment, such as the (4+2) coordination observed in the more covalently bonded II-VI and III-V compounds.

Note added in proof. We have recently become aware of a theoretical study[60] of the ordered binary analogue of the BC8 structure, which is adopted by CuCl-IV and CuBr-V. Their total energy pseudopotential calculations show this to be a stable structure in III-V semiconductors (such as GaAs, InAs, and AlSb) at elevated pressures. These high-pressure phases have not yet been observed experimentally except in the related I-VII compounds described here.

ACKNOWLEDGMENTS

We would like to thank W. I. F. David for valuable discussions concerning the work presented in this paper and C. N. Uden and T. Cooper for their assistance with the operation of the high-pressure cell.

[1]J. C. Phillips, Rev. Mod. Phys. **42**, 317 (1970).
[2]V. Meisalo and M. Kalliomäki, High Temp. High Pressures **5**, 663 (1973).
[3]G. J. Piermarini, F. A. Mauer, S. Block, A. Jayaraman, T. H. Geballe, and G. W. Hull, Jr., Solid State Commun. **32**, 275 (1979).
[4]N. R. Serebryanaya, S. V. Popova, and A. P. Rusakov, Sov. Phys. Solid State **17**, 1843 (1976).
[5]A. L. Edwards and H. G. Drickamer, Phys. Rev. **122**, 1149 (1961).
[6]A. van Valkenburg, J. Res. Nat. Bur. Std. **68A**, 97 (1964).
[7]H. Müller, S. Ves, H. D. Hochheimer, M. Cardona, and A. Jayaraman, Phys. Rev. B **22**, 1052 (1980); S. Ves, D. Glötzel, M. Cardona, and H. Overhof, Phys. Rev. B **24**, 3073 (1981).
[8]B. Batlogg, J. P. Remeika, and R. G. Maines, Solid State Commun. **38**, 83 (1981).
[9]A. Blacha, N. E. Christensen, and M. Cardona, Phys. Rev. B **33**, 2413 (1986).
[10]E. Rapoport and C. W. F. T. Pistorius, Phys. Rev. **172**, 838 (1968).
[11]J. M. Tranquada and R. G. Ingalls, Phys. Rev. B **34**, 4267 (1986).
[12]O. Brafman, M. Cardona, and Z. Vardeny, Phys. Rev. B **15**, 1081 (1977).
[13]S. Usha Devi and A. K. Singh, Pramana **17**, 461 (1981).
[14]M. J. Moore, J. S. Kasper, and F. P. Bundy, J. Solid State Chem. **1**, 170 (1970).
[15]S. Hull and D. A. Keen, Europhys. Lett. **23**, 129 (1993).
[16]L. Merrill, J. Phys. Chem. Ref. Data **6**, 1205 (1977).
[17]W. Klement, Jr. and A. Jayaraman, Prog. Solid State Chem. **3**, 289 (1966).
[18]E. F. Skelton, A. W. Webb, F. J. Rachford, P. C. Taylor, S. C. Yu, and I. L. Spain, Phys. Rev. B **21**, 5289 (1980).
[19]E. F. Skelton, S. B. Qadri, A. W. Webb, R. G. Ingalls, and J. M. Tranquada, Phys. Lett. **94A**, 441 (1983).
[20]N. B. Brandt, S. V. Kuvshinnikov, H. P. Rusakov, and M. V. Semenov, JETP Lett. **27**, 33 (1978).
[21]C. W. Chu, S. Early, T. H. Geballe, H. P. Rusakov, and R. Schwall, J. Phys. C **8**, L241 (1975).
[22]G. C. Vezzoli and J. Bera, Phys. Rev. B **23**, 3022 (1981).
[23]J. M. Besson, R. J. Nelmes, G. Hamel, J. S. Loveday, G. Weill, and S. Hull, Physica B **180&181**, 907 (1992).
[24]S. Hull, R. I. Smith, W. I. F. David, A. C. Hannon, J. Mayers, and R. Cywinski, Physica B **180&181**, 1000 (1992).
[25]W. I. F. David, R. M. Ibberson, and J. C. Matthewman (unpublished).
[26]P. J. Brown and J. C. Matthewman (unpublished).
[27]D. L. Decker, J. Appl. Phys. **42**, 3239 (1979).
[28]P. W. Bridgman, Proc. Acad. Arts Sci. **52**, 91 (1916).
[29]W. Mao-Chia Yang, L. H. Schwartz, and P. N. LaMori, J. Phys. Chem. Solids **29**, 1633 (1968).
[30]E. Hinze, High Temp. High Pressures **1**, 53 (1969).
[31]R. N. Kurdyumova and R. V. Baranova, Sov. Phys. Crystallogr. **6**, 318 (1961).
[32]R. Batchelor and T. Birchall, Acta Crystallogr. B **38**, 1260 (1982).
[33]P. A. Likforman, D. Carré, J. Etienne, and B. Batchet, Acta Crystallogr. B **31**, 1252 (1975).
[34]D. A. Keen and S. Hull, J. Phys. Condens. Matter **5**, 23 (1993).
[35]L. F. Vereschagin, W. B. White, and R. Roy, Science **137**, 993 (1962).
[36]J. D. Jorgensen and J. B. Clark, Phys. Rev. B **22**, 6149 (1980).
[37]E. I. Blount and J. C. Phillips, J. Less-Common Met. **62**, 457 (1978).
[38]V. P. J. Meisalo and M. S. Kalliomäki (unpublished).
[39]M. S. Kalliomäki (unpublished).
[40]K. J. Smolander, J. Phys. C **16**, 3673 (1983).
[41]A. Blacha and M. Cardona (unpublished results reported in Ref. 9).
[42]J. S. Kasper and S. M. Richards, Acta Crystallogr. **17**, 752 (1964).
[43]R. J. Nelmes, M. I. McMahon, N. G. Wright, D. R. Allan, and J. S. Loveday, Phys. Rev. B **48**, 9883 (1993).
[44]J. B. Clark and K. J. Range, Z. Naturforsch. B **31**, 158 (1976).
[45]K. E. Almin, Acta Chem. Scand. **2**, 400 (1948).
[46]F. Birch, J. Geophys. Res. **83**, 1257 (1978).
[47]R. C. Hanson, J. R. Halberg, and C. Schwab, Appl. Phys.

Lett. **21**, 490 (1972).
[48]S. N. Vaidya and G. C. Kennedy, J. Phys. Chem. Solids **32**, 951 (1971).
[49]J. Shanker, P. S. Bakhshi, and L. P. Sharma, J. Inorg. Nucl. Chem. **41**, 1285 (1979).
[50]A. Sadesh, A. Malillou, and B. R. K. Gupta, Phys. Status Solidi B **167**, K5 (1991).
[51]D. A. Keen and S. Hull, J. Phys. Condens. Matter **6**, 1637 (1994).
[52]W. Bührer and W. Hälg, Electrochim. Acta **22**, 701 (1977).
[53]G. Burley, Am. Mineral **48**, 1266 (1963); J. Phys. Chem. **68**, 1111 (1964).
[54]B. E. Mellander, J. E. Bowling, and B. Baranowski, Phys. Scr. **22**, 541 (1980); B. E. Mellander, Phys. Rev. B **26**, 5886 (1982).
[55]S. T. Weir, Y. K. Vohra, C. A. Vanderborgh, and A. L. Ruoff, Phys. Rev. B **39**, 1280 (1989).
[56]R. J. Nelmes, M. I. McMahon, P. D. Hatton, J. Crain, and R. O. Piltz, Phys. Rev. B **47**, 35 (1993).
[57]R. J. Nelmes, M. I. McMahon, N. G. Wright, and D. R. Allan, Phys. Rev. B **48**, 1314 (1993); M. I. McMahon, R. J. Nelmes, N. G. Wright, and D. R. Allan, Phys. Rev. B **48**, 16 246 (1993).
[58]J. R. Chelikowsky and J. K. Burdett, Phys. Rev. Lett. **56**, 961 (1986); J. R. Chelikowsky, Phys. Rev. B **35**, 1174 (1987); A. Mujica and R. J. Needs, Phys. Rev. B **48**, 17 010 (1993).
[59]N. E. Christensen, S. Satpathy, and Z. Pawlowska, Phys. Rev. B **36**, 1032 (1987).
[60]J. Crain, R. O. Plitz, G. J. Ackland, S. J. Clark, M. C. Payne, V. Milman, J. S. Lin, P. D. Hatton, and Y. H. Nam, Phys. Rev. B (to be published).

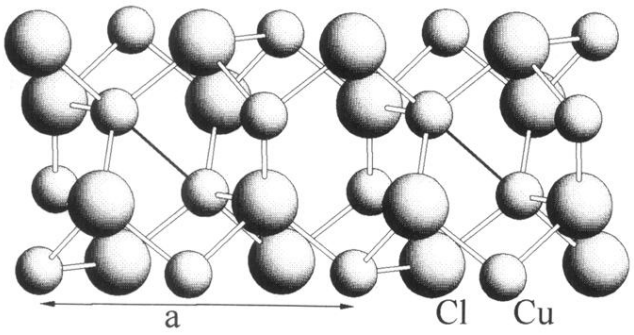

FIG. 10. The structure of the cubic $Pa\bar{3}$ phase of CuCl-IV. The approximately tetrahedral coordination of Cu^+ to four I^- is illustrated and the shorter Cu^+-Cu^+ distance is shown as a solid line.

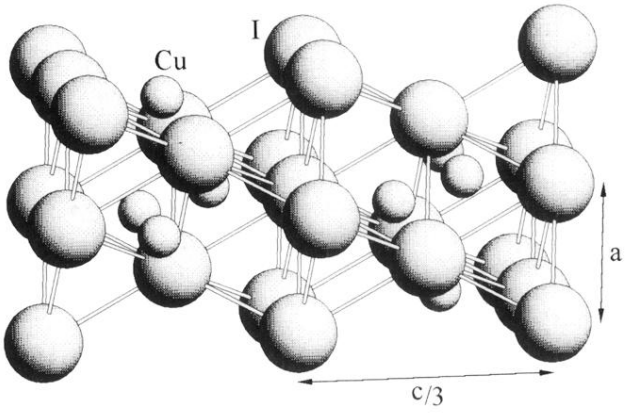

FIG. 5. The structure of the rhombohedral $R\bar{3}m$ phase of CuI-IV illustrating the location of the Cu^+ in the tetrahedral interstices of the almost regular cubic close-packed anion sublattice.

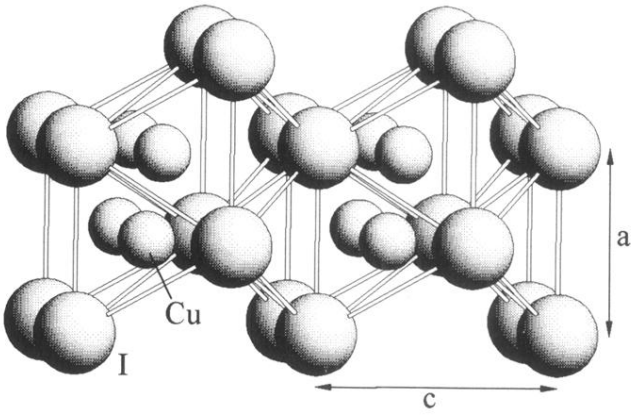

FIG. 7. The structure of the tetragonal *P4/nmm* phase of CuI-V. In this antilitharge structure the Cu^+ are located in the tetrahedral interstices of the almost regular cubic close-packed anion sublattice.